

# G-protein coupled receptor 56 promotes myoblast fusion through serum response factor- and nuclear factor of activated T-cell-mediated signalling but is not essential for muscle development *in vivo*

Melissa P. Wu<sup>1,2</sup>, Jamie R. Doyle<sup>3</sup>, Brenda Barry<sup>2,4</sup>, Ariane Beauvais<sup>2,\*</sup>, Anete Rozkalne<sup>2</sup>, Xianhua Piao<sup>5</sup>, Michael W. Lawlor<sup>6</sup>, Alan S. Kopin<sup>3</sup>, Christopher A. Walsh<sup>2,4</sup> and Emanuela Gussoni<sup>2</sup>

1 Department of Biological and Biomedical Sciences, Harvard Medical School, Boston, MA, USA

2 Division of Genetics, Boston Children's Hospital, MA, USA

3 Molecular Cardiology Research Institute, Tufts Medical Center, Boston, MA, USA

4 Howard Hughes Medical Institute, Boston Children's Hospital, MA, USA

5 Division of Newborn Medicine, Boston Children's Hospital, MA, USA

6 Department of Pathology and Laboratory Medicine, Children's Hospital of Wisconsin and Medical College of Wisconsin, Milwaukee, WI, USA

## Keywords

dystroglycanopathies; GPR56; myoblast; skeletal muscle; serum response element

## Correspondence

E. Gussoni, Division of Genetics, Boston Children's Hospital, Boston, MA 02115, USA

Fax: +1 617 730 0253

Tel: +1 617 919 2152

E-mail: gussoni@enders.tch.harvard.edu

## \*Present address

Department of Regenerative Medicine Program, Ottawa Hospital Research Institute, Ottawa, ON, Canada

(Received 1 July 2013, revised 24 August 2013, accepted 4 September 2013)

doi:10.1111/febs.12529

Mammalian muscle cell differentiation is a complex process of multiple steps for which many of the factors involved have not yet been defined. In a screen to identify the regulators of myogenic cell fusion, we found that the gene for G-protein coupled receptor 56 (GPR56) was transiently up-regulated during the early fusion of human myoblasts. Human mutations in the gene for GPR56 cause the disease bilateral frontoparietal polymicrogyria; however, the consequences of receptor dysfunction on muscle development have not been explored. Using knockout mice, we defined the role of GPR56 in skeletal muscle. GPR56<sup>-/-</sup> myoblasts have decreased fusion and smaller myotube sizes in culture. In addition, a loss of GPR56 expression in muscle cells results in decreases or delays in the expression of myogenic differentiation 1, myogenin and nuclear factor of activated T-cell (NFAT)c2. Our data suggest that these abnormalities result from decreased GPR56-mediated serum response element and NFAT signalling. Despite these changes, no overt differences in phenotype were identified in the muscle of GPR56 knockout mice, which presented only a mild but statistically significant elevation of serum creatine kinase compared to wild-type. In agreement with these findings, clinical data from 13 bilateral frontoparietal polymicrogyria patients revealed mild serum creatine kinase increase in only two patients. In summary, targeted disruption of GPR56 in mice results in myoblast abnormalities. The absence of a severe muscle phenotype in GPR56 knockout mice and human patients suggests that other factors may compensate for the lack of this G-protein coupled receptor during muscle development and that the motor delay observed in these patients is likely not a result of primary muscle abnormalities.

## Abbreviations

BFPP, bilateral frontoparietal polymicrogyria; CK, creatine kinase; DAPI, 4',6-diamidino-2-phenylindole; GPCR, G-protein coupled receptor; GPR56, G-protein coupled receptor 56; GPS, G-proteolytic site; H&E, haematoxylin and eosin; KO, knockout; MHC, myosin heavy chain; Myf5, myogenic factor 5; MyoD, myogenic differentiation 1; NFAT, nuclear factor of activated T-cells; PSG, penicillin/streptomycin/glutamine; shRNA, short-hairpin RNA; SRE, serum response element; SRF, serum response factor; tGPR56, truncated G-protein coupled receptor 56.

## Introduction

During muscle development, muscle progenitor cells in the somites migrate out to the limb buds and undergo two waves of myogenesis to form mature muscle [1]. This process of differentiation proceeds through several steps: progenitor cell proliferation and migration, the commitment to differentiation, myoblast–myoblast adhesion, and the fusion of cells to form syncytial myofibres [2]. These steps, largely recapitulated during adult muscle regeneration *in vivo* and myoblast differentiation *in vitro*, are regulated by the coordination of many factors. In particular, the ‘master’ transcription factors of the basic helix–loop–helix family direct myogenic differentiation in a sequential manner [3]. Precursor cells in the somites are specified to the myogenic lineage through the expression of the basic helix–loop–helix factor, myogenic factor 5 (Myf5) [4]. Myogenic differentiation 1 (MyoD) is expressed shortly after and also specifies myogenic precursor cells [5]. Although normally expressed in different cells [6,7], the loss of one can result in a compensatory up-regulation of the other [8,9]. After migration to the limb buds and exit from the cell cycle, the expression of myogenin induces myoblasts to differentiate [10]. Myogenin promotes the expression of factors that lead to cell–cell adherence and fusion, resulting in the formation of multinucleated myofibres.

Some of the cell-surface effectors of muscle cell differentiation and fusion have also been identified. Cell–cell adhesion molecules such as NCAM, N-cadherin, M-cadherin, ADAM12 and VCAM-1/VLA-4 are involved in cell–cell adhesion of muscle cells [2]. Other proteins have also been implicated as being important for fusion, although their specific roles remain unclear. Part of the difficulty in identifying the role of cell surface proteins is that many of them act cooperatively and/or in parallel, thus complementing the functions of each other [11]. A complete understanding of the molecular regulation of muscle development awaits a more complete characterization of these molecules, as well as the identification of the other as yet unknown factors that are involved.

A previous study suggested that GPR56 expression is up-regulated during the early differentiation of myoblasts [12]. Pull-down assays demonstrated that GPR56 localizes to a tetraspanin microdomain specified by the tetraspanins CD81 and CD9, which are associated with the  $G\alpha_{q/11}$  subunit [13]. CD81 and CD9 have each been implicated as partners that promote the fusion of myoblasts [14]. GPR56 expression has been associated with the migration and adhesion of neural progenitor cells, gliomas, and melanoma cells [15–21], which are processes that are also important for the differentiation of myoblasts into multinucleated myotubes.

GPR56 belongs to the adhesion subfamily of G-protein coupled receptors, which are characterized by their large extracellular *N*-terminal structure and a GPCR proteolytic site: a G-proteolytic site (GPS) motif [22]. The GPS site is auto-catalytically cleaved during protein translation through the action of a GPCR–auto-proteolysis inducing domain that encompasses both the GPS motif and regions *N*-terminal to it [23]. The resulting extracellular *N*-terminal fragment and membrane-bound *C*-terminal fragment then re-associate with each other noncovalently at the cell surface [24–26]. Recessive mutations in GPR56 that result in the loss of GPR56 protein at the surface of the cell, particularly those that disturb the cleavage of the GPS domain, cause the rare neurodevelopmental disease bilateral frontoparietal polymicrogyria (BFPP; OMIM #606854) [27,28]. Patients with BFPP are characterized by mental retardation, motor developmental delays, seizures, and defects in the brainstem and cerebellum [27,29–33]. The defects in the brainstem and cerebellum manifest through the development of polymicrogyria, which are aberrantly small convolutions on the brain surface [34]. Patients with the muscle dystroglycanopathies, in particular muscle–eye–brain disease and Walker–Warburg Syndrome, also display these ‘cobblestone’ brain abnormalities [34,35] in addition to developing severe muscular dystrophies [36–38]. Given the overlap in brain abnormalities seen in these diseases, there has been speculation regarding the potential role of GPR56 in skeletal muscle.

Accordingly, we have conducted studies using GPR56 knockout mice, silencing RNA in a differentiating myoblast cell line (i.e. in C2C12 cells), as well as luciferase assays to explore receptor-mediated signalling. We found that GPR56 is transiently up-regulated in myocytes (differentiated myoblasts that have not yet fused) and nascent myotubes. This increase follows the induction of MyoD expression and is concurrent with myogenin expression. A loss of GPR56 results in decreased myoblast fusion in culture. Our data suggest that this abnormality may reflect decreased receptor-mediated serum response factor (SRF) and nuclear factor of activated T-cell (NFAT) signalling. Despite the disruption of GPR56-mediated pathways, no differences in myofibre size or fibre type specification were detected in GPR56 knockout mice. In a study of regenerating muscle, GPR56 knockout (KO) mice showed delays in the expression of MyoD and myogenin. Analysis of serum creatine kinase (CK) levels revealed a mild but statistically significant increase in GPR56 knockout mice compared to

wild-type. This finding was consistent with the clinical data obtained from 13 BFPP patients, where only two patients exhibited elevated serum CK levels. In summary, our data suggest that GPR56 supports the activation of serum response element (SRE) and NFAT signalling, which in turn promotes myoblast differentiation but not myofibre hypertrophy or fibre type specification. The lack of a muscle phenotype in GPR56 knockout mice suggests that other factors may compensate for the lack of GPR56 during muscle development. Therefore, the motor delay observed in BFPP patients is not likely caused by a primary muscle defect.

## Results

### GPR56 is transiently expressed during muscle cell differentiation

To define the timing of GPR56 expression, primary mouse myoblasts were isolated and induced to differentiate by serum withdrawal. At various times throughout differentiation, mRNA and protein lysates were collected (Fig. 1A–C). Both GPR56 mRNA (Fig. 1B) and protein (Fig. 1C) are transiently induced

during the early fusion of primary mouse myoblasts (D1, D2) and quickly down-regulated during later fusion stages. GPR56 protein expression in myoblast cultures follows the onset of MyoD expression and is concomitant with myogenin expression (Fig. 1C), suggesting that GPR56 is present in post-mitotic myocytes committed to fusion.

The myoblast cultures at D1 and D2, where GPR56 expression is the highest, contain a mixture of proliferating and quiescent myoblasts, committed myocytes and early myotubes with few nuclei. To determine which of these cells were expressing GPR56, we performed immunofluorescence staining on myoblasts at D1 (Fig. 1D,E and S1). GPR56 was detected in mononuclear cells, some of which were in close association with myotubes (Fig. 1D, arrows). There was also slight immunoreactivity in myotubes, particularly surrounding the nuclei. The cultures were co-stained with caveolin-1, which is expressed in myoblasts but not myocytes [39], aiming to better distinguish whether the GPR56-positive mononuclear cells were in myoblasts or myocytes (Fig. 1D,E). The cells did not co-express GPR56 and caveolin-1, suggesting that GPR56 is only expressed in differentiating myocytes.

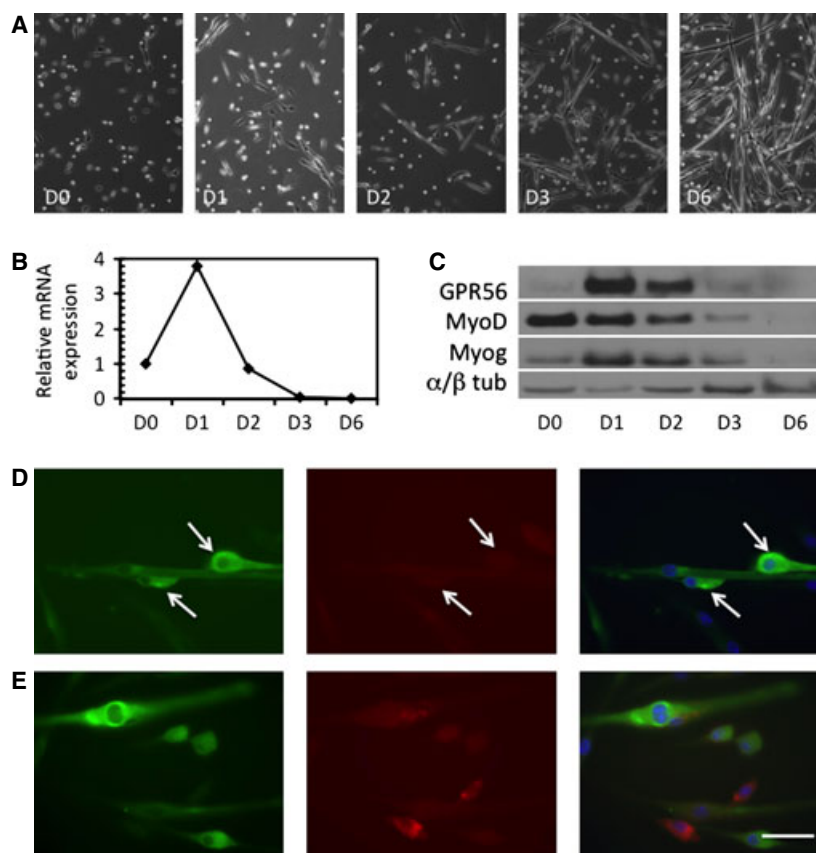


**Fig. 1.** GPR56 is transiently expressed in the early differentiation phase of mouse myoblasts. (A) Phase images of mouse myoblasts induced to differentiate over the course of 6 days (D0–D6) indicating the degree of myotube formation. (B) Up-regulation of GPR56 mRNA expression at D1 by quantitative RT-PCR in primary mouse myoblasts which then rapidly decreases. (C) Protein expression of GPR56, MyoD, myogenin and  $\alpha/\beta$ -tubulin (loading control) in myoblasts at D0–D6, as assessed by western blotting. GPR56 protein expression peaks at D1 and rapidly decreases by D3, where little expression remains. (D, E) GPR56 (green) and caveolin-1 (red) staining in differentiating primary mouse myoblasts at D1. DAPI (blue) was used to stain nuclei. Arrows point to GPR56<sup>+</sup> cells that are positioned closely and elongated, suggesting that the cells are readying for fusion or fusing. Scale bar = 50  $\mu$ m.

### Loss of GPR56 results in decreased myoblast fusion through decreases in SRE and NFAT activity

To determine the role of GPR56 during myoblast differentiation, GPR56 was silenced using two separate short-hairpin RNA (shRNA) constructs in the mouse C2C12 myoblast cell line (Fig. 2A). Both GPR56 shRNA constructs efficiently silenced GPR56 mRNA and protein expression (Fig. 2B,C). MyoD expression did not appear to be dramatically altered in GPR56-silenced C2C12 cultures, whereas myogenin expression was decreased, particularly with shRNA construct 3. Myoblast fusion and myotube size were significantly decreased in the GPR56-silenced C2C12 cells at day 5 after the induction of differentiation (Fig. 2D–F).

Multiple transcriptional pathways are involved in the early differentiation of myoblasts into myocytes and small myotubes *in vitro*. In particular, evidence that GPR56 downstream signalling includes the activation of the SRE and NFAT-response element (NFAT-RE) in gene promoters has been reported [40]. The SRE DNA element is functionally equivalent to the CARG box in myogenic cells [41] to which the SRF binds. To confirm that GPR56 activates the SRE and NFAT-RE, we used vectors expressing full-length GPR56 (mGPR56) and a constitutively active variant, which includes an N-terminal GPR56 truncation (tGPR56) [26]. We assessed how the expression of these constructs activated either an SRE or NFAT-RE luciferase reporter gene (Fig. 2G). Truncated GPR56 activated both the SRE and NFAT reporters, whereas

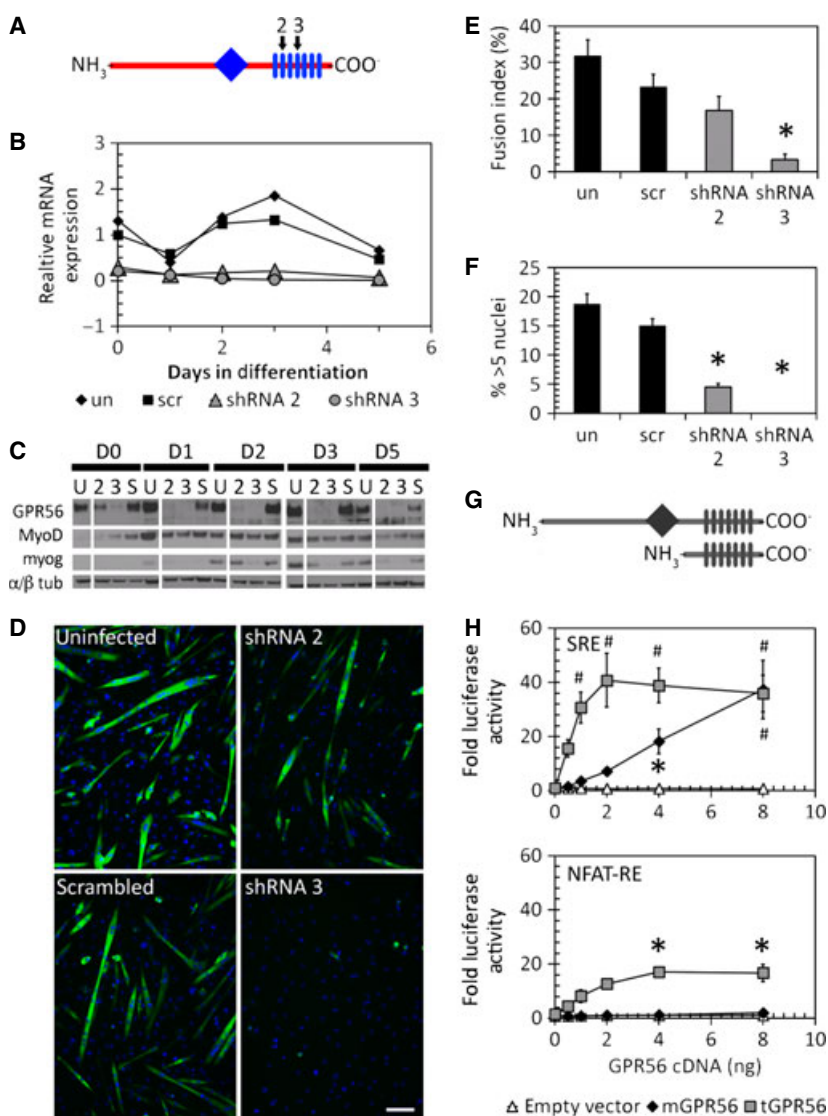


**Fig. 2.** GPR56 is involved in directing myoblast fusion through SRF and NFAT pathways. (A) Schematic diagram showing the location of GPR56 shRNA constructs (2, 3, black arrows) against GPR56 transmembrane domains (rectangles) 2 and 4. The diamond indicates the G-proteolytic site. (B) GPR56 mRNA expression by quantitative RT-PCR in silenced C2C12s. Both shRNA2 and 3 effectively silenced the expression of GPR56. (C) Western blotting of GPR56, MyoD and myogenin proteins in silenced C2C12 cells. (D) MHC staining in GPR56-silenced cultures shows decreased myotube formation in GPR56 shRNA2 and 3 silenced cells. Scale bar = 50  $\mu$ m. (E) Fusion is decreased in GPR56-silenced cells at day 5 after differentiation. Un, uninfected; scr, scrambled oligo. \* $P < 0.01$ . (F) Myotube size is decreased in GPR56-silenced cells at day 5 after differentiation. \* $P < 0.01$ . un, uninfected; scr, scrambled oligo. (G) Schematic showing full-length and truncated GPR56. Diamond, G proteolytic site; rectangles, transmembrane domains. (H) Luciferase reporter assays in HEK293 cells of full-length (mGPR56; black diamond) or truncated (tGPR56; grey squares) GPR56 with luciferase reporter constructs driven by SRE or NFAT-RE. GPR56 induces signalling from both SRE and NFAT-RE. \* $P < 0.05$ . # $P < 0.001$  ( $n = 3$ ).

the full-length receptor activated only the SRE luciferase construct (Fig. 2H).

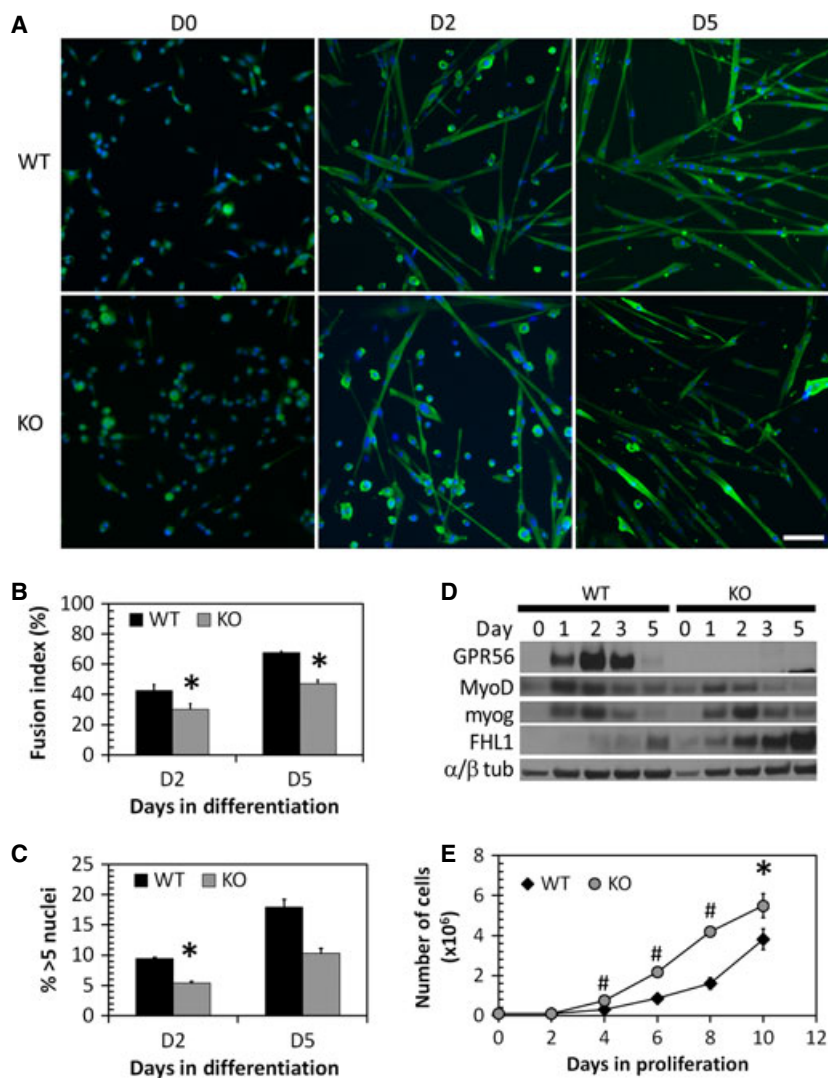
### Primary myoblasts from GPR56-knockout mice exhibit decreased differentiation and fusion

To extend our findings to an *in vivo* model, primary myoblasts were isolated from littermate wild-type and GPR56 knockout mice. Myoblasts were FACS-sorted from dissociated limb and back muscles [42], differentiated for 5 days and analyzed for their fusion competence (Fig. 3). Knockout myoblasts exhibited a decreased ability to fuse, as indicated by their fusion index at days 2 and 5 in differentiation media (Fig. 3A,B). Quantification of the myotube size demonstrates that knockout cells also form smaller myotubes at D2 (Fig. 3C), whereas, by D5, the myotube size is not significantly different between knockout and

wild-type cultures. The ability of the knockout myotubes to grow to sizes similar to those of wild-type myotubes by D5 suggests that GPR56 plays a role only in the early stages of myoblast fusion.

To more precisely define GPR56 function in relation to myogenic differentiation, we looked at the protein expression of myogenic transcription factors (Fig. 3D). Decreases in signalling to the SRF transcription factor could result in reduced expression of the downstream transcription factors MyoD and myogenin, which regulate differentiation [43–45]. Indeed, MyoD expression appeared to be decreased at days 3 and 5 in the differentiating knockout compared to wild-type myoblasts at similar time points, whereas there was no change in the early marker of differentiation, myogenin. To confirm whether NFAT signalling was altered, we examined the expression of the transcriptional co-activator, FHL1, which supports NFATc1 and NFATc2 in promoting

**Fig. 3.** GPR56 knockout myoblasts fuse less and have decreased MyoD expression. (A) Wild-type and GPR56 knockout mouse myoblasts undergoing differentiation at D0, D2 and D5. Scale bar = 50  $\mu$ m. Green, desmin (D0) or MHC (D2, D5). Blue, nuclei. (B) Fusion index in wild-type and knockout differentiating mouse myoblasts. GPR56 knockout myoblasts have decreased fusion at D2 and D5. \* $P < 0.05$  ( $n = 4$ ). (C) Overall myotube size as measured by the percentage of myotubes with more than five nuclei in wild-type and knockout differentiating cultures. \* $P < 0.05$ . (D) Protein expression by western blotting of GPR56, MyoD, myogenin and  $\alpha/\beta$ -tubulin in differentiating myoblasts at D0–D5. GPR56 knockout myoblasts show decreased MyoD expression at days 3 and 5, and increased FHL1 expression. (E) GPR56 knockout myoblasts (grey circles) proliferate more than wild-type myoblasts (black diamonds). \* $P \leq 0.05$ , # $P < 0.001$  ( $n = 4$ ).



myoblast fusion and myotube growth after the onset of myogenin expression [46–48]. FHL1 was up-regulated in the differentiating knockout myoblast cultures (Fig. 3D).

Additionally, GPR56 knockout primary myoblasts proliferated significantly faster than wild-type myoblasts over the course of 10 days (Fig. 3E). These data support the conclusion that a loss of GPR56 results in less efficient commitment of myoblasts to differentiation, which manifests as decreased fusion ability *in vitro*.

### GPR56 knockout muscle is morphologically normal

Mutations in GPR56 result in the human genetic disease BFPP. Patients with BFPP share similarities in brain pathology with dystroglycanopathy patients (Fig. 4A) who also exhibit severe muscle defects, particularly muscular dystrophy [34]. Some patients with BFPP have a motor delay or early muscle hypotonia, resulting in the consideration of congenital myopathy or muscular dystrophy as a diagnosis [33,49]. These parallels suggest that BFPP patients may also have a specific muscle defect. A review of serum CK levels in 13 BFPP patients revealed that two patients had slightly elevated values (Fig. 4B). Given that muscle biopsies for these patients were not available, muscle from GPR56 knockout mice was analyzed. The gastrocnemius and tibialis anterior muscles of 1–3-month-old wild-type and knockout mice were examined after haematoxylin and eosin (H&E) staining (Fig. 4C). They revealed no signs of myopathy or dystrophy, such as fibrosis, necrosis or increased fibre size heterogeneity. To determine whether the *in vitro* myoblast fusion defect translated to decreased myofibre size *in vivo*, the myofibre sizes of knockout versus wild-type mouse gastrocnemius muscle were quantified. This analysis revealed no significant difference (Fig. 4D). However, we found a slight but statistically significant increase in the serum CK levels of GPR56 knockout mice compared to wild-type mice ( $n = 11–12$  mice per group;  $P = 0.012$ ; Fig. 4E).

The GPR56-downstream signalling pathways that were altered in differentiating myogenic cells were also analyzed for their expression in the muscle. MyoD, a transcriptional target of SRF signalling during myoblast commitment and differentiation [43,44,50], has decreased mRNA expression in GPR56 knockout muscle compared to wild-type muscle (Fig. 4F); this decrease is in agreement with the MyoD protein expression data in differentiating muscle cells (Fig. 3D). Similarly, the expression of NFAT family members that are involved in commitment and early myoblast fusion are also affected in GPR56 knockout mice. NFATc3

activity supports MyoD-directed myogenesis [51,52], whereas NFATc2 is activated in early myotubes [46]. The mRNA expression of both NFATc2 and NFATc3 were significantly down-regulated in GPR56 knockout muscle (Fig. 4F). In addition, FHL1, whose transcription is also under the control of SRE [53], exhibited decreased expression in knockout mouse muscle (Fig. 4F). These decreases in mRNA expression suggest that both SRE and NFAT signalling pathways are altered in GPR56 knockout mouse muscle.

### The fusion defects seen *in vitro* do not translate to defective muscle regeneration *in vivo*

To determine whether the decreased fusion and myotube size seen *in vitro* translated into reduced myofibre size during muscle regeneration, the tibialis anterior muscles of wild-type and knockout mice were injured by injection with cardiotoxin (Fig. 5). GPR56 mRNA expression in regenerating wild-type muscle is transiently increased and peaks at day 4 after cardiotoxin injection (Fig. 5B). Morphologically, there was no gross defect in the timing or extent of regeneration in knockout compared to wild-type muscle (Fig. 5A). There was also no significant difference in myofibre diameter 4 days after cardiotoxin injection between knockout and wild-type muscle (Fig. 5C). At 6 and 18 days, there were no differences in myofibre diameter (Fig. 5C).

We then examined the expression of critical myogenic transcription factors in the regenerating wild-type and knockout muscles. In knockout mice, the peaks in Myf5 and MyoD expression were delayed (Fig. 5D). The timing of later stages of myofibre nuclear accretion as indicated by the expression of NFATc2, FHL1 and embryonic myosin heavy chain (MHC), however, appeared to match the timing in wild-type mice. Overall, although some of the molecular determinants of myoblast differentiation were significantly different or delayed in expression in the knockout muscle compared to wild-type, muscle regeneration did not appear to be affected.

The NFAT signalling pathways activated during myoblast commitment and differentiation are also used to regulate fibre type differentiation [54,55]. Because the loss of GPR56 in knockout mice affected these pathways during muscle cell differentiation, we examined whether myofibre type specification was altered in the gastrocnemius muscle at various ages. No differences in protein expression between wild-type and GPR56 knockout mouse muscles were detected by western blotting using antibodies specific to MHC type I, IIA and IIB (Fig. 5E,F). We also used immunofluorescence to manually count the individual myofibres

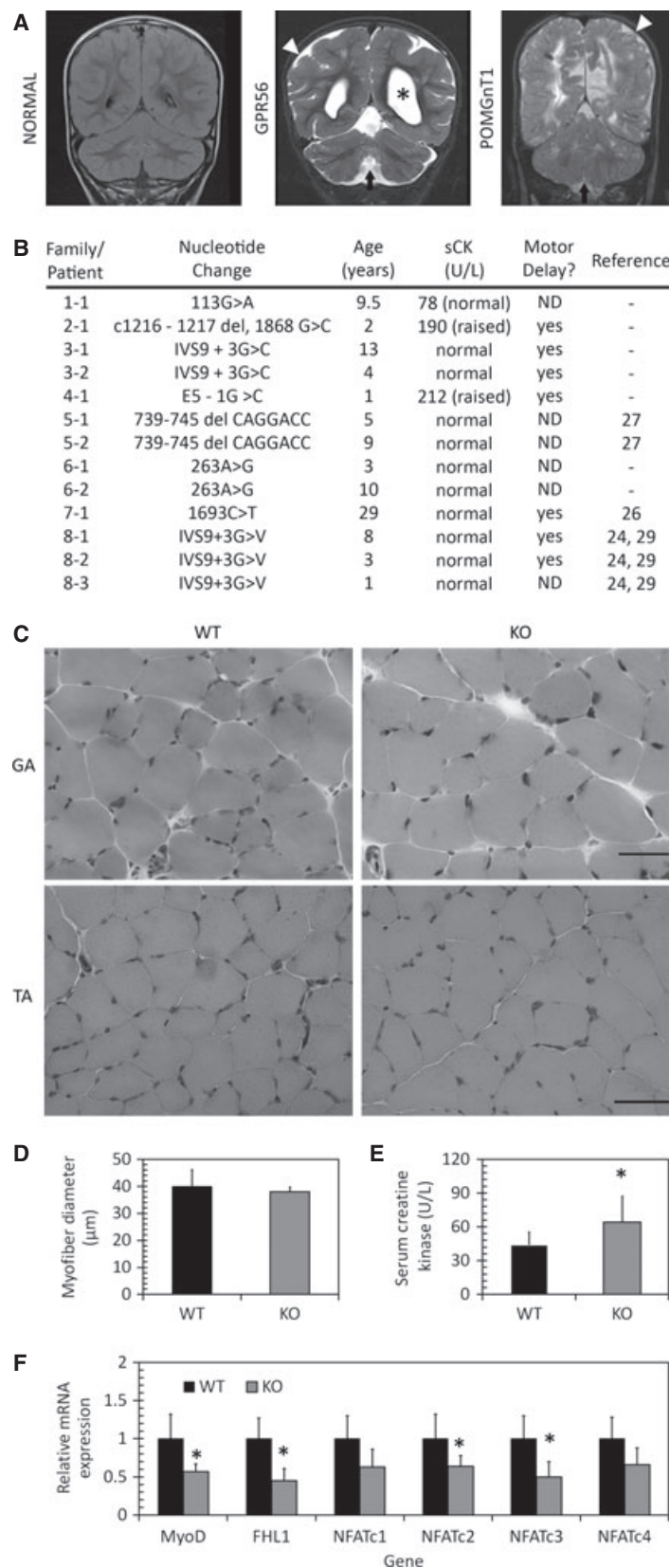


**Fig. 4.** Muscle phenotypes in BFPP patients and GPR56 knockout mice. (A) Representative coronal flair magnetic resonance image from an unaffected individual (NORMAL) and coronal T2 images from individuals with confirmed mutations in GPR56 and POMGnT1. Patients exhibit enlarged ventricles (asterisks), the presence of diffused cortical abnormalities (white arrowhead) and the presence of cerebellar abnormalities, including a small vermis in the GPR56 patient (arrow). (B) Serum CK levels and motor developmental delays in patients with BFPP. ND, not determined. (C) H&E staining of 1-month-old gastrocnemius (top, GA) and tibialis anterior (bottom, TA) muscles shows no difference between wild-type and knockout muscle. Scale bars = 50  $\mu\text{m}$ . (D) Myofibre diameter in tibialis anterior muscle shows no difference between wild-type and knockout muscle. (E) Serum CK levels in wild-type and knockout mice shows slightly elevated serum CK levels in knockout mice. \* $P = 0.012$  ( $n = 11-12$ ). (F) mRNA expression in wild-type and knockout gastrocnemius muscle. Expression of MyoD, FHL1, NFATc2 and NFATc3 are decreased in knockout muscle. \* $P < 0.05$  ( $n = 6$ ).

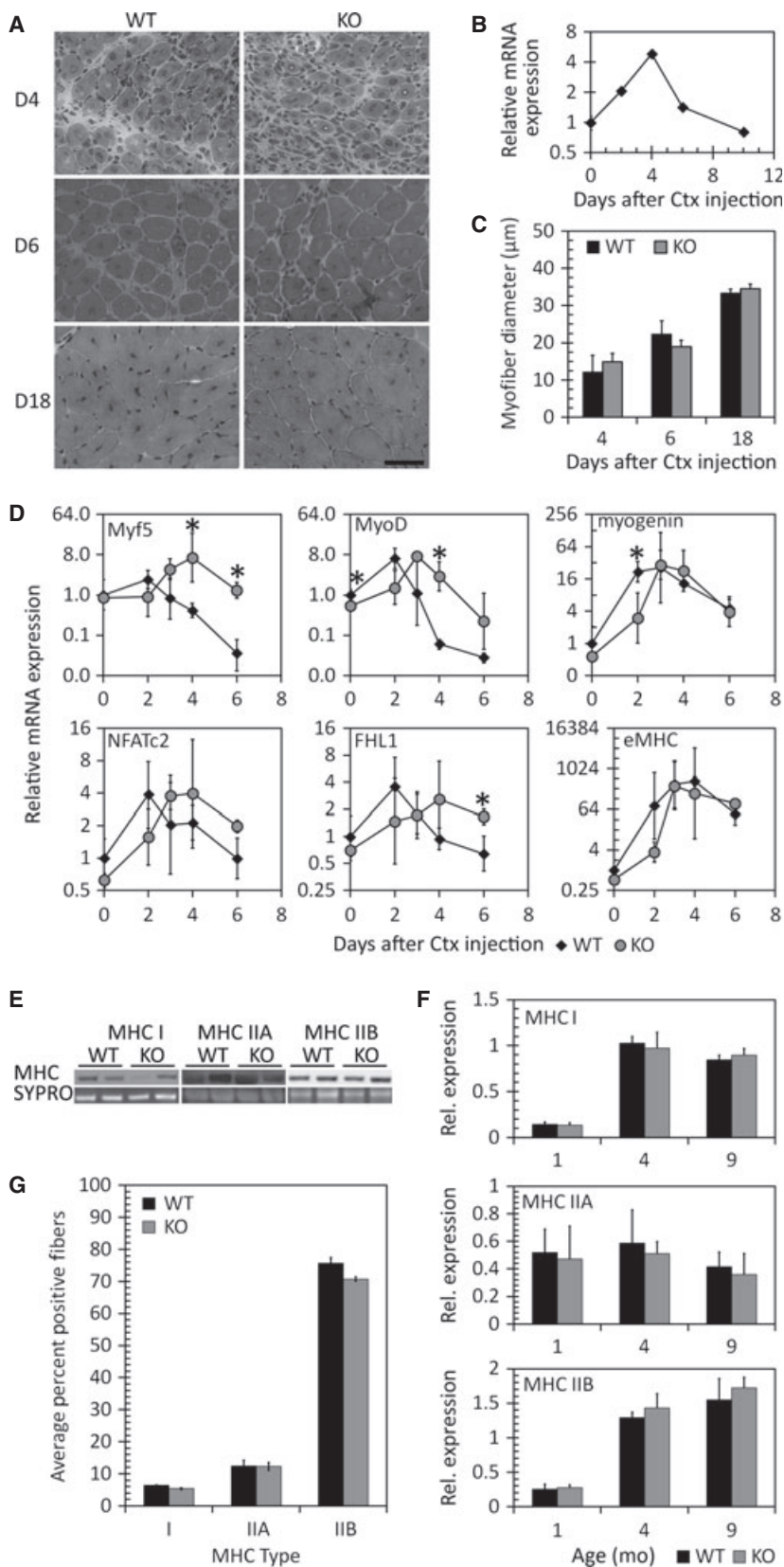


**Fig. 5.** Loss of GPR56 affects the expression of myogenic transcription factors during regeneration but does not affect myofiber size. (A) H&E staining of GPR56 wild-type and knockout gastrocnemius muscle at days 4, 6 and 18 after cardiotoxin injury. Knockout morphology and timing does not look different from wild-type. (B) mRNA expression of GPR56 by quantitative RT-PCR shows transient up-regulation of GPR56 during regeneration. (C) Myofiber diameter in cardiotoxin-injured wild-type and GPR56 knockout gastrocnemius muscle shows no difference in diameter between wild-type and knockout. (D) mRNA expression by quantitative RT-PCR of various genes in wild-type (black diamond) and GPR56 knockout (grey circle) cardiotoxin-injured muscle. Myf5, MyoD and myogenin are delayed in expression in knockout muscle.  $*P < 0.05$  ( $n = 3$ ). (E) Sample western blots of MHC protein expression. (F) Quantification of the amount of MHC I, IIA or IIB protein expression by western blotting in wild-type and knockout gastrocnemius muscle in mice of various ages shows no difference in the amount of MHC isoforms between wild-type and knockout. (G) Quantification of the percentage of positive MHC I, IIA or IIB fibre types in knockout versus wild-type muscles, based on immunofluorescence staining in four littermate pairs.

and ensure that the lack of differences in MHC expression detected by western blotting was not a result of a lack of sensitivity (Fig. 5G and S2). We isolated the gastrocnemius muscle from 1-month-old littermates, stained sequential sections with antibodies against MHC I, IIA or IIB together with anti-laminin to outline the myofibres, and quantified the proportion of positive myofibres for each MHC type. No differences in the proportion of fibre types were found between wild-type and knockout muscle (Fig. 5G). Thus, although GPR56 signals through the SRF and NFAT pathways, it does not affect the NFAT-directed specification of fibre types.

## Discussion

Mutations in GPR56 result in the human disease BFPP [27,33,56]. The similarities in brain phenotype between BFPP and the dystroglycanopathies have resulted in their classification as similar diseases [34,49]. These diseases are caused through a loss of binding between cell membrane proteins and the extracellular matrix ( $\alpha$ -dystroglycan to laminin [57,58] and GPR56 to collagen III [21]), which suggests a shared disease mechanism. We previously found that GPR56 is up-regulated in differentiating human fetal muscle cells [12], suggesting that its loss could affect muscle cell differentiation and result in a muscle phenotype. Thus, we investigated the role of GPR56 in the skeletal muscle using the GPR56 knockout mouse in conjunction with cell-based assays.

Our *in vitro* studies delineate a role for GPR56 in the commitment of myoblasts to early differentiation. GPR56 localizes to myocytes and nascent myotubes, whereas the luciferase assays link GPR56 expression with the activation of promoters containing the SRF DNA-binding elements. These data together with the previous findings demonstrating that GPR56 activates RhoA [17,21,26], draw a possible pathway for GPR56 at the cell surface to activate RhoA signalling and subsequently activate the SRF-mediated transcription of target genes in the nuclei of myoblasts committed to differentiation.

Our findings that full-length and truncated mouse GPR56 can activate luciferase driven by SRE agree with a previous study showing that different human isoforms of GPR56 were able to activate SRE-driven luciferase to varying degrees [40]. In myoblasts, the SRF transcription factor binds an SRE DNA element within the MyoD promoter to promote the transcription of MyoD during proliferation and differentiation [43,44,50]. The activation of SRF transcriptional activity, in turn, is dependent on RhoA [50]. The

up-regulation of MyoD expression, in correlation with a switch in SRF phosphorylation [59], induces proliferating myoblasts to exit the cell cycle [5]. MyoD then switches to a differentiation programme to prepare the cells for fusion. The inhibition of SRF expression or activity has been shown to lead to decreased MyoD [50] and myogenin expression [60]. In support of these possible signalling links between GPR56, SRF and MyoD, we observed a decrease in MyoD mRNA expression in GPR56 knockout muscle, as well as decreases in MyoD and myogenin expression in differentiating GPR56 knockout and GPR56-silenced C2C12 myoblasts, respectively. Satellite cells lacking MyoD continue to proliferate and inefficiently express myogenin when induced to differentiate [61,62]; in our studies, GPR56 knockout myoblasts showed increased proliferation rates compared to wild-type myoblasts. These data support the conclusion that GPR56 might signal through the SRF to promote transcription of the myogenic regulators of myoblast commitment to differentiation (i.e. MyoD).

This transcriptional programme of myogenic differentiation is aided by many cofactors, including NFATc3. NFATc3 potentiates the ability of MyoD to activate the myogenic differentiation programme [51]. NFATc2 is then activated in the nascent myotubes to promote further fusion [46]. Our data demonstrate that a loss of GPR56 resulted in significantly decreased NFATc3 and NFATc2 expression. In our luciferase assays, constitutively-active GPR56 stimulated NFAT transcription to a lesser degree than SRE transcription. One of the target genes of the SRF is FHL1 [45,53], a co-activator of NFAT transcription in the muscle [48]. Increased FHL1 expression was seen in GPR56 knockout myoblasts but not in GPR56-silenced C2C12 cells. This inconsistency suggests that GPR56 activation of NFAT-RE is not direct but, instead, occurs via the induction of FHL1 transcription after activation of the SRF.

Clearly, the *in vitro* loss of GPR56 negatively affected the ability of myoblasts to efficiently differentiate and fuse, although these effects did not alter muscle development or regeneration *in vivo*. The initial examination of GPR56 knockout muscle histology found no gross changes in muscle histology or myofibre size. We did, however, find a small but statistically significant increase in the serum CK levels, which indicates the presence of myofibre membrane damage, as seen in muscular dystrophy [63,64]. However, in the case of GPR56 knockout mice, the degree of serum CK elevation was much smaller than that seen in a mouse model of the dystroglycanopathies [65]. That the increase was slight, albeit significant, is in agreement with other studies that did

not detect raised serum CK levels in BFPP patients [49] and with our findings of two patients with only slightly elevated serum CK. Therefore, the loss of GPR56 in human muscle did not lead to a severe phenotype in this tissue.

After acute injury, GPR56 knockout muscle regenerated normally although the expression of Myf5 and MyoD were delayed. The overall mild phenotype *in vivo* suggests that GPR56 could be one of many factors that promote commitment and differentiation and that the redundancy in function with other genes can compensate for its loss. Myf5 is known to be able to compensate for loss of MyoD [6,8,9] and its delayed but emphatic increase during regeneration may act as a compensatory mechanism for the less efficient expression of MyoD in GPR56 knockout muscle. This hypothesis is supported by our *in vitro* findings that, despite a significantly decreased ability of GPR56 knockout myoblasts to fuse at early time points, the myotube sizes were not different from wild-type myotube sizes at later time points (D6). In addition, the fusion defect was more prominent in the GPR56-silenced C2C12 cells, as opposed to the primary GPR56 knockout myoblasts. Because the knockout myoblasts develop in a GPR56-null environment and were isolated from postnatal muscle, it is possible that they adapted their differentiation mechanisms to compensate for the loss of GPR56. These compensatory mechanisms would not have had time to develop in GPR56-silenced C2C12 cells and could be one reason for why the phenotype of silenced cells was more severe than in primary knockout cells.

In skeletal muscle, four major myofibre types can be classified by their MHC contractile abilities [66]. Type I fibres have slow MHCs, whereas Types IIA, IIX and IIB have fast MHCs. Intrinsic and extrinsic factors lead to the specification, maintenance and switching of a particular fibre type [67]. *in vivo* RNA silencing of different NFATs shows that fibre type specification is influenced and dictated by different combinations of four isoforms of NFAT (c1 to c4) [55]. All four NFAT isoforms studied play roles in maintaining the Type I fibre type, whereas only NFATc2 through NFATc4 are required for Type IIA and Type IIX fibres, and only NFATc4 for Type IIB fibres. In the present study, despite decreases in NFATc2 and NFATc3 expression in GPR56 knockout mice, no differences in fibre type specification were seen in GPR56 knockout mouse muscle. These findings agree with reports that knockouts of the NFAT family members have little to no effect on fibre type specification [46,52] and support our conclusion that GPR56 signalling through NFAT

is likely to be important only during the early stages of fusion.

Despite a clear role for GPR56 in myoblast commitment and differentiation, there are several reasons why its loss may not severely impact muscle function in BFPP patients and GPR56-null mice. GPR56 expression is transient and restricted to early differentiation in both myoblasts in culture and regenerating muscle *in vivo*. It has been suggested that cell-surface molecules with roles in myoblast differentiation exhibit less severe phenotypes when individually knocked-out in mice as a result of redundancy in their functions [11]. Although the functions of  $\alpha$ -dystroglycan and GPR56 in brain development appear to be similar, the relative importance of their ligands may differ in the brain versus skeletal muscle. A clear role for the importance of  $\alpha$ -dystroglycan binding to laminin has been established in both tissues [68–70]. Although laminin is a major component of the mature muscle basal lamina [71], the ligand collagen III of GPR56 is expressed only transiently during development [72]. Similarly,  $\alpha$ -dystroglycan is an integral component of the dystrophin-associated protein complex, which is expressed in both developing and mature muscle, whereas GPR56 is expressed transiently. Thus, although in the brain,  $\alpha$ -dystroglycan and GPR56 serve similar functions with respect to aiding neuronal cell migration, in skeletal muscle, their pattern of expression and downstream signalling pathways are clearly distinct. These studies demonstrate that, although loss of GPR56 function in myogenic cells leads to decreased ability to fuse as a result of altered signalling through SRF, skeletal muscle development is not affected overall.

## Materials and methods

### Human subjects

Clinical details on patients and families affected by *GPR56* mutations and other neurological conditions were obtained with written consent as part of their participation in research studies at Boston Children's Hospital and Beth Israel Deaconess Medical Center. The studies were approved by the Internal Review Board at each participating institution and performed in accordance with the ethical standards covering human subjects research.

### Animals

GPR56 knockout mice (B6N.129S5-*Gpr56*<sup>tm1Lex</sup>/Mmcd) were generated by Genentech/Lexicon Genetics (South San Francisco, CA, USA). The absence of GPR56 protein was verified previously [18]. Animals were euthanized by CO<sub>2</sub>

asphyxiation and the appropriate muscles dissected. Unless otherwise stated, tissue was collected from 1-month-old male animals.

For evaluation of serum CK levels, mice between 5 and 10 months of age were nicked in the tail vein and 200  $\mu\text{L}$  blood was collected. Blood was allowed to coagulate for 1 h at room temperature and then centrifuged at 16 100  $g$  in a table-top microfuge for 1.5 min. Twenty microlitres of plasma serum were used in the CK-NAC (UV-Rate) CK test (#0910; Stanbio Laboratory, Boerne, TX, USA) to determine serum CK levels. For each blood sample, two measurements were taken and averaged. A total of 11 wild-type and 12 knockout animals were analyzed. Data were analyzed for statistical significance using Student's *t*-test (unpaired, homoscedastic) in EXCEL (Microsoft Corp., Redmond, WA, USA) with  $P < 0.05$  considered statistically significant. Error bars represent the SD between samples.

For cardiotoxin injections, mice ( $n = 5$ ) were anaesthetized with isoflurane and a total of 15  $\mu\text{L}$  of 0.5  $\mu\text{g}\cdot\text{mL}^{-1}$  cardiotoxin (#C9759-5MG; Sigma-Aldrich, St Louis, MO, USA) in NaCl/Pi was injected into three different sites in the right tibialis anterior with a Hamilton syringe (26-G needle). Mice were sacrificed at 2, 3, 4, 6 and 18 days after cardiotoxin injury. Left (uninjured) tibialis anterior muscles were used as uninjured (D0) controls.

For tissue section analyses, tissue was snap-frozen by embedding in OCT (Tissue-Tek #4583; VWR, Arlington Heights, IL, USA) in liquid nitrogen-cooled isopentane. For mRNA and protein analyses, tissue was snap-frozen in liquid nitrogen. All animals were handled in accordance with protocols approved by the Institutional Animal Care and Use Committee at Boston Children's Hospital.

### H&E staining and determination of myofibre diameter

For myofibre diameter analysis, 1- $\mu\text{m}$  sections of tibialis anterior muscle tissue were taken from the approximate belly of the muscle. For cardiotoxin-injured muscle, sections were taken from the injured area. Tissue sections were stained as described previously [73] and imaged using a E1000 microscope (Nikon, Tokyo, Japan) with a SPOT Insight Color 3.2.0 camera using SPOT, version 4.5.9.9 (Spot Imaging Solutions; Diagnostic Instruments Inc, Sterling Heights, MI, USA).

Fibre diameter was measured using IMAGEJ, version 1.4 (NIH, Bethesda, MD, USA) and the plug-in 'Measure and Label.java'. For cardiotoxin-injured muscle, only fibres with centrally-located nuclei were measured. For each mouse, fibre diameter measurements within two to three fields were averaged. Approximately 140 fibres were counted per field, totalling 280–420 fibres per mouse. Each data bar represents the measurements of three to five mice. Error bars represent the SD between the measurements for the mice. Significance was determined using an unpaired Student's *t*-test.

### Determination of fibre type proportions by immunohistochemistry

Sequential 10- $\mu\text{m}$  muscle cross-sections from the approximate centre of 1-month-old littermate wild-type and knockout gastrocnemius muscle were fixed in cold 100% acetone for 5 min and then air-dried for 20 min. They were then washed with  $1 \times \text{NaCl/P}_i\text{-T}$  (0.1% Tween-20 in NaCl/P<sub>i</sub>) and blocked for 30 min in 2.5% horse serum in NaCl/P<sub>i</sub>-T. Sections were then incubated overnight at 4 °C in primary antibody in NaCl/P<sub>i</sub>-T using the MHC type antibodies MHC1 (dilution 1 : 100; #M8421; Sigma-Aldrich); mouse anti-MHC Type IIA (dilution 1 : 50; Developmental Studies Hybridoma Bank, Iowa City, IA, USA; #SC-71, developed by S. Schiaffino; or mouse anti-MHC Type IIB (dilution 1 : 50; Developmental Studies Hybridoma Bank; #BF-F3, developed by S. Schiaffino) and co-stained with a rabbit anti-laminin antibody (dilution 1 : 100; #L9393; Sigma-Aldrich) to outline the myofibres. After three 3-min washes in NaCl/P<sub>i</sub>-T, slides were incubated for 1 h at room temperature with the appropriate secondary antibody in NaCl/P<sub>i</sub>-T, washed three times in NaCl/P<sub>i</sub>-T and mounted with 4',6-diamidino-2-phenylindole (DAPI) Vectashield (#H-1200; Vector Laboratories, Burlingame, CA, USA).

The entire section was photographed in sequential fields using a Orca-ER camera (#C4742-95-12ER; Hamamatsu, Middlesex, NJ, USA) mounted on a Zeiss Axioplan 2 microscope ( $\times 5$  objective) with AXIOVISION, version 4.5 SP1 (Carl Zeiss, Oberkochen, Germany). The individual fields were merged together into one image using PHOTOSHOP CS3 (Adobe Systems, San Jose, CA, USA). The numbers of MHC-positive and negative fibres in each section were manually counted using the cell counter function in IMAGEJ, version 1.4 (NIH). Significance was determined using Student's *t*-test (paired) in EXCEL (Microsoft Corp.) with  $P < 0.05$  considered statistically significant. Error bars represent the SE of measurement between samples.

### Primary myoblast isolation, proliferation and fusion assays

Limb skeletal muscles from littermate wild-type and GPR56 knockout mice were dissected, minced and dissociated with 5  $\text{mg}\cdot\text{mL}^{-1}$  collagenase D (#11088882001; Roche Applied Science, Indianapolis, IN, USA) and 5  $\text{mg}\cdot\text{mL}^{-1}$  dispase II (#04942078001; Roche Applied Science) per gram of tissue for up to 1 h at 37 °C. After dissociation, filtration through 100- and 40- $\mu\text{m}$  filters and red blood cell removal (#158904; Qiagen, Valencia, CA, USA), myogenic cells were isolated by FACS as described previously [42]. Myoblasts were then plated on 6-cm plastic plates coated with 5  $\mu\text{g}\cdot\text{cm}^{-2}$  collagen type I (#354236; BD Biosciences, Franklin Lakes, NJ, USA) in myoblast growth media (30% fetal bovine serum and  $1 \times$  penicillin/streptomycin/glutamine (PSG) in 1 : 1 F10/high-glucose DMEM)

supplemented with  $10 \text{ ng}\cdot\text{mL}^{-1}$  basic fibroblast growth factor (#X07995; Atlanta Biologicals, Norcross, GA, USA).

For proliferation assays, myoblasts were plated at  $1 \times 10^4$  cells on collagen-coated 12-well plates. Every 2 days for up to 10 days, duplicate wells of myoblasts were trypsinized and counted. The total number of cells was then calculated for each sample. Comparisons were made using a paired Student's *t*-test. Error bars show the SE among experimental sets. Data are represented as the mean of three trials.

For fusion assays,  $2 \times 10^5$  myoblasts were plated on gel-coated six-well dishes in myoblast growth media +  $10 \text{ ng}\cdot\text{mL}^{-1}$  basic fibroblast growth factor. The next day (D0), they were switched to differentiation media (2% horse serum/1  $\times$  PSG in low-glucose DMEM), which was changed daily for up to 6 days. To assess fusion, cells were fixed with 4% paraformaldehyde in NaCl/P<sub>i</sub> for 15 min at room temperature, and washed with NaCl/P<sub>i</sub>; the nuclei were then stained with DAPI in NaCl/P<sub>i</sub>. Images of cells were taken using a Photometrics CoolSNAP EZ camera (Photometrics, Tucson, AZ, USA) mounted on a Eclipse TE2000-S microscope (Nikon) with NIS ELEMENTS AR 2.30 SP4 software (Nikon). Fusion was analyzed using the cell counter function in IMAGEJ, version 1.4 or 1.47b (NIH). For each sample, three fields were taken and the results were averaged per duplicate or triplicate well. Each field contained approximately 100–200 nuclei, depending on the day of fusion. The fusion index was calculated as:  $100 \times (\text{total number of nuclei in myotubes})/(\text{total number of nuclei})$ . The mean myotube size was calculated as:  $(\text{total number of nuclei in myotubes})/(\text{total number of myotubes counted})$ . For these counts, myotubes were defined as cells containing two or more nuclei. The final results are the mean of each experiment with four total experiments comprising three sets of littermate mouse myoblast isolations. Comparisons between wild-type and knock-out were made using a paired Student's *t*-test with  $P < 0.05$  considered statistically significant. Error bars show the SE among experimental sets.

For immunostaining, myoblasts were fixed with 4% paraformaldehyde in NaCl/P<sub>i</sub> for 15 min and permeabilized with 1% Triton X-100/PBS for 3 min. After washing with NaCl/P<sub>i</sub>, cells were blocked in 10% fetal bovine serum/0.1% Triton X-100 in NaCl/P<sub>i</sub> for 1 h at room temperature. Cells were then treated with 1% SDS for 1 min and rinsed three times for 5 min in NaCl/P<sub>i</sub>. Cells were then incubated mouse anti-GPR56 (dilution 1 : 100; #SAB1400340; Sigma) and rabbit anti-caveolin-1 (dilution 1 : 200; #3238; Cell Signaling, Danvers, MA, USA) in blocking buffer overnight at 4 °C. After washing three times with NaCl/P<sub>i</sub>, cells were incubated with secondary antibody (Dylight 488 anti-mouse IgG and Dylight 594 anti-rabbit IgG; Jackson ImmunoResearch Laboratories, West Grove, PA, USA; #715-486-150 and #711-516-152, respectively) in blocking buffer for 1 h at room temperature. After incubation, cells were washed three times with

NaCl/P<sub>i</sub>, and mounted with DAPI Vectashield. Cells were imaged with an Orca-ER camera mounted on a Nikon E1000 microscope with OPENLAB, version 5.5.0 software (Improvision; PerkinElmer, Waltham, MA, USA).

### C2C12 cell gene silencing and fusion assays

Short hairpin oligos were designed against mouse GPR56 mRNA (accession number: [NM\\_018882](#)) and annealed into the BD RNAi-Ready pSiren-RetroQ viral vector (#631526; BD Biosciences Clontech, Mountain View, CA, USA). The sequences used were: shRNA2, 5'-TCACGTGACTACAC CATCA-3' and shRNA3, 5'-CGTTGGTGGATGTGAAT AA-3'. 293GP cells were plated in 10% fetal bovine serum/1  $\times$  PSG in DMEM and transfected the next day with 8  $\mu\text{g}$  of vesicular stomatitis virus-G plasmid and 8  $\mu\text{g}$  of silencing or control vector using a standard calcium phosphate protocol. Twelve to 16 h after transfection, the media (containing virus) was collected and filtered through a 0.45- $\mu\text{m}$  polyethersulfone low-protein binding filter to remove cell debris.

The viral infection followed a protocol based on Springer *et al.* [74]. The viral suspension was supplemented with 20% fetal bovine serum and 8  $\text{ng}\cdot\text{uL}^{-1}$  polybrene (final concentrations). The viral mix was added to C2C12s (plated the previous day on gel-coated six-well plates at  $7 \times 10^4$  cells), incubated for 15 min in a cell culture incubator (37 °C, 5% CO<sub>2</sub>) and spun at 1100 *g* for 30 min at 32 °C. The viral mix was then removed and replaced with fresh C2C12 growth media (20% fetal bovine serum, 1  $\times$  PSG in high-glucose DMEM). Cells were re-infected with this protocol at 8, 16 and 24 h after the first infection. The efficiency of infection was verified in parallel infections with virus carrying the pQCLIN construct, which confirmed that 95–100% of C2C12 cells expressed LacZ (data not shown).

Infected C2C12 cells were switched to differentiation media 6 h after the last infection, and assayed for fusion and mRNA and protein profiles as described below. The D0 timepoint was taken just before switching the media to differentiation. Subsequent time points were taken at D1, D2, D3 and D5 for mRNA and protein, and D2 and D5 for the fusion assay. The fusion index and myotube size were assayed as with the primary myoblasts, with the mean of ten fields taken per single well per sample per trial. The final results are the averaged results from three independent viral infections. Comparisons between GPR56-silenced samples and control samples were made using one-way analysis of variance (ANOVA) from STATPLUS:MAC LE (Analyst Soft Inc., Alexandria, VA, USA). Error bars show the SE among experimental sets.

For immunostaining, cells were fixed and stained as with the primary myoblasts, without 1% SDS treatment. The primary antibody used was mouse anti-myosin (dilution 1 : 100; Developmental Studies Hybridoma Bank; #MF-20, developed by D. A. Fischman).

### RNA isolation from cells and tissue, reverse transcription and quantitative RT-PCR

For cultured cells, cells were trypsinized and pelleted. RNA was isolated using the RNeasy Mini kit (#74104; Qiagen).

For tissues, RNA was isolated using the RNeasy Fibrous Tissue kit (#74704; Qiagen) with modifications. Approximately 10 mg of snap-frozen tissue was homogenized in 650  $\mu$ L of RLT + 1%  $\beta$ -mercaptoethanol (v/v) with Lysing Matrix D beads (#6913; MP Bio, Solon, OH, USA) in a Fastprep FP120 homogenizer (Thermo Savant Qbiogene, Inc., Carlsbad, CA, USA) for two cycles of 40 s at speed 6, with a 5-min incubation on ice inbetween. Homogenized tissue was then spun down at 4 °C at 16 100 *g* for 4 min, and 300  $\mu$ L of the supernatant containing the RNA was transferred to an eppendorf tube. Ten microlitres of proteinase K solution and 590  $\mu$ L of RNase-free water was then added, and the sample was incubated for 10 min at 55 °C. The subsequent RNA isolation steps with DNA removal were carried out in accordance with the manufacturer's instructions.

cDNA was reverse-transcribed from 0.5 to 2  $\mu$ g of RNA using either the Quantitect Reverse Transcription kit (#205311; Qiagen) or the Superscript III Reverse Transcription kit (#18080-051; Invitrogen Life Technologies, Grand Island, NY, USA) with a mix of random hexamers and oligoT primers. For each experimental set, the same kit was used. From this reaction, 1 : 40 to 1 : 20 volume (0.5–1  $\mu$ L) of cDNA was amplified using SYBR green (#4364346; Invitrogen Life Technologies) and quantified in a 7900HT Fast Real-Time PCR System (Applied Biosystems Life Technologies, Grand Island, NY, USA). Relative expression was calculated using the  $\Delta\Delta C_t$  method [75]. All primers were optimized to run at the same efficiency as control primers ( $\beta$ 2-microglobulin for cell and uninjured muscle assays or GAPDH for cardiotoxin injury assays) [76]. Primers were designed to span exon–intron junctions and/or large introns. All assays were run with no template and minus reverse transcriptase controls. The primers used are listed in Table S1.

### Protein isolation and western blot analysis

Cells were lysed directly on the plate with RIPA cell lysis buffer (50 mM Tris, pH 7.4, 150 mM NaCl, 1% NP-40, 1 mM EDTA) with 0.1% SDS, protease inhibitor cocktail (#4693159001; Roche Applied Science) and phosphatase inhibitor cocktail (#4906837001; Roche Applied Science). Lysates were collected and rotated for 1 h at 4 °C, then centrifuged at 16 100 *g* for 25 min at 4 °C. The supernatant and pellet were separated.

Snap-frozen tissue samples were crushed into a powder using a liquid-nitrogen cooled ceramic mortar and pestle. An aliquot of the powder was taken and homogenized in TPER buffer (#78510; Thermo Scientific, Pittsburg, PA, USA) with 0.1% SDS/protease inhibitor cocktail/phosphatase inhibitor

cocktail for 1 min at 4 °C, using a hand-held homogenizer and plastic pestles. Samples were then rotated at 4 °C for 1 h and frozen at –20 °C to complete lysis. After thawing, samples were centrifuged and the supernatant aliquoted.

One to 20  $\mu$ g of protein per sample was prepared with NuPage LDS loading buffer (#NP0007; Invitrogen Life Sciences, Carlsbad, CA, USA) and 5%  $\beta$ -mercaptoethanol (v/v); samples were then denatured for 10 min at 65 °C before loading onto 4–12% Bis-Tris gels (#WG1402BOX; Invitrogen Life Sciences). Proteins were transferred to nitrocellulose for 1 h in transfer buffer (12.5 mM Tris-glycine, pH 8.3, 10% methanol). Blots were blocked in 5% BSA/1% milk in TBST (25 mM Tris, 3 mM KCl, 140 mM NaCl, 0.01% Tween-20) for 1 h at room temperature and incubated in primary antibody in blocking buffer overnight at 4 °C on a shaker. For detecting GPR56, blots were blocked and incubated with primary antibody in 5% BSA/2% milk/TBST. After three washes with TBST, blots were incubated with the appropriate horseradish peroxidase-conjugated secondary antibodies (dilution 1 : 10 000; Jackson ImmunoResearch Laboratories) in 5% milk in TBST for 40 min at room temperature. Bands were detected using the Western Lightning chemiluminescent detection reagent (#NEL105001EA; Perkin Elmer, Boston, MA, USA). After detection, blots were stripped for 25 min at 80 °C in stripping buffer (0.2 M glycine, pH 2.5, 0.05% Tween-20), washed for 1 h in TBST and re-probed for other proteins. The primary antibodies used were: mouse anti-mouse GPR56 (dilution 1 : 1000; H11 clone; generous gift from Xianhua Piao, Boston Children's Hospital, Boston, MA, USA), mouse anti-MyoD (dilution 1 : 1000; #554130; BD Biosciences), mouse anti-myogenin (dilution 1 : 1000; Developmental Studies Hybridoma Bank; #F5D, developed by F. W. Wright), goat anti-FHL1 (dilution 1 : 1000; #Ab23937; Abcam, Cambridge, MA, USA), rabbit anti-GAPDH 14C10 (dilution 1 : 1000; #2118; Cell Signaling) and rabbit anti- $\alpha$ / $\beta$ -tubulin (dilution 1 : 5000; #2148; Cell Signaling). For the analysis of primary mouse myoblasts, protein lysates from four sets of myoblasts isolated from littermate wild-type and knockout mice were analyzed. For the analysis of silenced C2C12 cells, protein lysates were made from three sets of C2C12 cells that were independently infected.

For quantification of MHC types, the total protein on replicate nitrocellulose blots was stained with SYPRO Ruby Protein Blot Stain (#S-11791; Invitrogen Life Sciences). Bands were imaged using the Bio-Rad Chemidoc XRS+ molecular imaging system and densitometry readings were taken using the volume rectangle tool in QUANTITY ONE, version 4.6.2 (Bio-Rad, Hercules, CA, USA). The blots were destained and then blotted for either mouse anti-slow MHC (dilution 1 : 1000; #M8421; Sigma-Aldrich), mouse anti-MHC Type IIA (dilution 1 : 1000; Developmental Studies Hybridoma Bank; #SC-71) or mouse anti-MHC Type IIB (dilution 1 : 1000; Developmental Studies Hybridoma

Bank; #BF-F3). Multiple ECL readings of the MHC bands were taken using the Bio-Rad Chemidoc XRS+ to ensure the collection of an unsaturated exposure. The densitometry measurements for MHC bands were normalized to the total protein SYPRO bands, and the results from three to five mice were averaged. Significance was determined using an unpaired Student's *t*-test in EXCEL. Error bars show the SD between samples.

### Luciferase assays

The mouse GPR56 coding sequence (accession number: [NM\\_018882](#)) was amplified from a V5-tagged mouse GPR56 construct kindly provided by Samir Koirala (Boston Children's Hospital, Boston, MA, USA) [19]. Constitutively active, tGPR56 [26] was cloned into pCMV-XL4 by amplifying the C-terminal domain of GPR56 after the GPS cleavage site. The location of the GPS cleavage site was determined by homology to GPS sites found in other adhesion GPCRs [77]. The forward primers incorporated *NotI* restriction enzyme sites, a Kozak initiation sequence, and a methionine amino acid translational start site: full-length GPR56 (mGPR56) forward primer 5'-AAGCGGCCGCC ACCATGGCTGTCCAGGTGCTG-3' and tGPR56 forward primer 5'-AAGCGGCCGCCACCATGACCTACTT TGCAGTGCTGAT-3'. The reverse primer incorporated a *NotI* restriction enzyme site after the stop codon and was used for both mGPR56 and tGPR56: 5'-TTGCGGCCGCT GCAGAATTGCCCTAGATGC-3'.

HEK293 cells were plated in 96-well plates at a density of 6000 cells/well, 1 day before transfection, or 3000 cells/well, 2 days before transfection, in 10% fetal bovine serum/DMEM. Cells were transfected using Lipofectamine (#18324-012; Invitrogen Life Sciences) with: (a) 0–8 ng of mGPR56-pCMV-XL4, tGPR56-pCMV-XL4 or pCMV-XL4 empty vector control; (b) 20 ng of SRE<sub>5x</sub>-luc or NFAT-RE-luc reporter; and (c) 5 ng of  $\beta$ -galactosidase pcDNA1.1 control in serum-free DMEM. Luciferase and  $\beta$ -galactosidase activity were assayed as described previously [78]. Averaged triplicate data for each experiment were normalized to basal signalling from cells transfected with reporter and  $\beta$ -galactosidase alone. Data from three separate experiments were averaged to produce the normalized relative luciferase activity. Significance was analyzed by two-way analysis of variance with Bonferroni correction in GRAPHPAD PRISM, version 5 (GraphPad Software Inc., San Diego, CA, USA). Error bars denote the SE among experiments.

### Acknowledgements

This work was supported by the National Institutes of Health (2R01NS047727 and 1R01AR060317-01 to E.G.; T32 GM007226 to M.P.W., K08 AR059750 and L40 AR057721 to M.W.L.; and NIH-P30-HD1865 to the Boston Children's Hospital Stem Cell Core

Facility). The antibodies against MHC Type IIA and MHC Type IIB, developed by S. Schiaffino, were obtained from the Developmental Studies Hybridoma Bank developed under the auspices of the NICHD and maintained by The University of Iowa (Department of Biology, Iowa City, IA, USA). We are grateful to Isabelle Draper for numerous helpful discussions. We also extend our thanks to Marie Torres in the Stem Cell Core Facility, Boston Children's Hospital and Suzan Lazo-Kallanian at the Hematologic Neoplasia Core Facility, Dana Farber Cancer Institute, for help with the FACS isolation of primary myoblasts; Ci Chen for cell plating at Tufts Medical Center; and Chelsea Cherenfant, Hui Meng and Alexandra Lerch-Gaggl for help with the myofibre type analysis. The authors declare that they have no conflicts of interest.

### References

- Buckingham M, Bajard L, Chang T, Daubas P, Hadchouel J, Meilhac S, Montarras D, Rocancourt D & Relaix F (2003) The formation of skeletal muscle: from somite to limb. *J Anat* **202**, 59–68.
- Abmayr SM & Pavlath GK (2012) Myoblast fusion: lessons from flies and mice. *Development* **139**, 641–656.
- Lassar AB, Skapek SX & Novitch B (1994) Regulatory mechanisms that coordinate skeletal muscle differentiation and cell cycle withdrawal. *Curr Opin Cell Biol* **6**, 788–794.
- Ott MO, Bober E, Lyons G, Arnold H & Buckingham M (1991) Early expression of the myogenic regulatory gene, *myf-5*, in precursor cells of skeletal muscle in the mouse embryo. *Development* **111**, 1097–1107.
- Halevy O, Novitch BG, Spicer DB, Skapek SX, Rhee J, Hannon GJ, Beach D & Lassar AB (1995) Correlation of terminal cell cycle arrest of skeletal muscle with induction of p21 by MyoD. *Science* **267**, 1018–1021.
- Braun T & Arnold HH (1996) Myf-5 and myoD genes are activated in distinct mesenchymal stem cells and determine different skeletal muscle cell lineages. *EMBO J* **15**, 310–318.
- Kablar B, Krastel K, Ying C, Asakura A, Tapscott SJ & Rudnicki MA (1997) MyoD and Myf-5 differentially regulate the development of limb versus trunk skeletal muscle. *Development* **124**, 4729–4738.
- Rudnicki MA, Braun T, Hinuma S & Jaenisch R (1992) Inactivation of MyoD in mice leads to up-regulation of the myogenic HLH gene Myf-5 and results in apparently normal muscle development. *Cell* **71**, 383–390.
- Rudnicki MA, Schnegelsberg PN, Stead RH, Braun T, Arnold HH & Jaenisch R (1993) MyoD or Myf-5 is required for the formation of skeletal muscle. *Cell* **75**, 1351–1359.

- 10 Wright WE, Sassoon DA & Lin VK (1989) Myogenin, a factor regulating myogenesis, has a domain homologous to MyoD. *Cell* **56**, 607–617.
- 11 Krauss RS (2010) Regulation of promyogenic signal transduction by cell–cell contact and adhesion. *Exp Cell Res* **316**, 3042–3049.
- 12 Cerletti M, Molloy MJ, Tomczak KK, Yoon S, Ramoni MF, Kho AT, Beggs AH & Gussoni E (2006) Melanoma cell adhesion molecule is a novel marker for human fetal myogenic cells and affects myoblast fusion. *J Cell Sci* **119**, 3117–3127.
- 13 Little KD, Hemler ME & Stipp CS (2004) Dynamic regulation of a GPCR-tetraspanin-G protein complex on intact cells: central role of CD81 in facilitating GPR56-Galpha q/11 association. *Mol Biol Cell* **15**, 2375–2387.
- 14 Tachibana I & Hemler ME (1999) Role of transmembrane 4 superfamily (TM4SF) proteins CD9 and CD81 in muscle cell fusion and myotube maintenance. *J Cell Biol* **146**, 893–904.
- 15 Shashidhar S, Lorente G, Nagavarapu U, Nelson A, Kuo J, Cummins J, Nikolich K, Urfer R & Foehr ED (2005) GPR56 is a GPCR that is overexpressed in gliomas and functions in tumor cell adhesion. *Oncogene* **24**, 1673–1682.
- 16 Ke N, Sundaram R, Liu G, Chionis J, Fan W, Rogers C, Awad T, Grifman M, Yu D, Wong-Staal F *et al.* (2007) Orphan G protein-coupled receptor GPR56 plays a role in cell transformation and tumorigenesis involving the cell adhesion pathway. *Mol Cancer Ther* **6**, 1840–1850.
- 17 Iguchi T, Sakata K, Yoshizaki K, Tago K, Mizuno N & Itoh H (2008) Orphan G protein-coupled receptor GPR56 regulates neural progenitor cell migration via a G alpha 12/13 and Rho pathway. *J Biol Chem* **283**, 14469–14478.
- 18 Li S, Jin Z, Koirala S, Bu L, Xu L, Hynes RO, Walsh CA, Corfas G & Piao X (2008) GPR56 regulates pial basement membrane integrity and cortical lamination. *J Neurosci* **28**, 5817–5826.
- 19 Koirala S, Jin Z, Piao X & Corfas G (2009) GPR56-regulated granule cell adhesion is essential for rostral cerebellar development. *J Neurosci* **29**, 7439–7449.
- 20 Xu L, Begum S, Barry M, Crowley D, Yang L, Bronson RT & Hynes RO (2010) GPR56 plays varying roles in endogenous cancer progression. *Clin Exp Metastasis* **27**, 241–249.
- 21 Luo R, Jeong SJ, Jin Z, Strokes N, Li S & Piao X (2011) G protein-coupled receptor 56 and collagen III, a receptor-ligand pair, regulates cortical development and lamination. *Proc Natl Acad Sci USA* **108**, 12925–12930.
- 22 Lin HH, Stacey M, Yona S & Chang GW (2010) GPS proteolytic cleavage of adhesion-GPCRs. *Adv Exp Med Biol* **706**, 49–58.
- 23 Arac D, Boucard AA, Bolliger MF, Nguyen J, Soltis SM, Sudhof TC & Brunger AT (2012) A novel evolutionarily conserved domain of cell-adhesion GPCRs mediates autoproteolysis. *EMBO J* **31**, 1364–1378.
- 24 Krasnoperov VG, Bittner MA, Beavis R, Kuang Y, Salnikow KV, Chepurny OG, Little AR, Plotnikov AN, Wu D, Holz RW *et al.* (1997) alpha-Latrotoxin stimulates exocytosis by the interaction with a neuronal G-protein-coupled receptor. *Neuron* **18**, 925–937.
- 25 Nechiporuk T, Urness LD & Keating MT (2001) ETL, a novel seven-transmembrane receptor that is developmentally regulated in the heart. ETL is a member of the secretin family and belongs to the epidermal growth factor-seven-transmembrane subfamily. *J Biol Chem* **276**, 4150–4157.
- 26 Paavola KJ, Stephenson JR, Ritter SL, Alter SP & Hall RA (2011) The N terminus of the adhesion G protein-coupled receptor GPR56 controls receptor signaling activity. *J Biol Chem* **286**, 28914–28921.
- 27 Piao X, Hill RS, Bodell A, Chang BS, Basel-Vanagaite L, Straussberg R, Dobyns WB, Qasrawi B, Winter RM, Innes AM *et al.* (2004) G protein-coupled receptor-dependent development of human frontal cortex. *Science* **303**, 2033–2036.
- 28 Jin Z, Tietjen I, Bu L, Liu-Yesucevitz L, Gaur SK, Walsh CA & Piao X (2007) Disease-associated mutations affect GPR56 protein trafficking and cell surface expression. *Hum Mol Genet* **16**, 1972–1985.
- 29 Harbord MG, Boyd S, Hall-Craggs MA, Kendall B, McShane MA & Baraitser M (1990) Ataxia, developmental delay and an extensive neuronal migration abnormality in 2 siblings. *Neuropediatrics* **21**, 218–221.
- 30 Dobyns WB, Patton MA, Stratton RF, Mastrobattista JM, Blanton SH & Northrup H (1996) Cobblestone lissencephaly with normal eyes and muscle. *Neuropediatrics* **27**, 70–75.
- 31 Straussberg R, Gross S, Amir J & Gadoth N (1996) A new autosomal recessive syndrome of pachygyria. *Clin Genet* **50**, 498–501.
- 32 Farah S, Sabry MA, Khuraibet A, Khaffagi S, Rudwan M, Hassan M, Haseeb N, Abulhassan S, Abdel-Rasool MA, Elgamel S *et al.* (1997) Lissencephaly associated with cerebellar hypoplasia and myoclonic epilepsy in a Bedouin kindred: a new syndrome? *Clin Genet* **51**, 326–330.
- 33 Piao X, Chang BS, Bodell A, Woods K, Benzeev B, Topcu M, Guerrini R, Goldberg-Stern H, Sztriha L, Dobyns WB *et al.* (2005) Genotype–phenotype analysis of human frontoparietal polymicrogyria syndromes. *Ann Neurol* **58**, 680–687.
- 34 Barkovich AJ, Millen KJ & Dobyns WB (2009) A developmental and genetic classification for midbrain-hindbrain malformations. *Brain* **132**, 3199–3230.

- 35 Quattrocchi CC, Zanni G, Napolitano A, Longo D, Cordelli DM, Barresi S, Randisi F, Valente EM, Verdolotti T, Genovese E *et al.* (2013) Conventional magnetic resonance imaging and diffusion tensor imaging studies in children with novel GPR56 mutations: further delineation of a cobblestone-like phenotype. *Neurogenetics* **14**, 77–83.
- 36 Michele DE, Barresi R, Kanagawa M, Saito F, Cohn RD, Satz JS, Dollar J, Nishino I, Kelley RI, Somer H *et al.* (2002) Post-translational disruption of dystroglycan-ligand interactions in congenital muscular dystrophies. *Nature* **418**, 417–422.
- 37 Kim DS, Hayashi YK, Matsumoto H, Ogawa M, Noguchi S, Murakami N, Sakuta R, Mochizuki M, Michele DE, Campbell KP *et al.* (2004) POMT1 mutation results in defective glycosylation and loss of laminin-binding activity in alpha-DG. *Neurology* **62**, 1009–1011.
- 38 Jimenez-Mallebrera C, Torelli S, Feng L, Kim J, Godfrey C, Clement E, Mein R, Abbs S, Brown SC, Campbell KP *et al.* (2009) A comparative study of alpha-dystroglycan glycosylation in dystroglycanopathies suggests that the hypoglycosylation of alpha-dystroglycan does not consistently correlate with clinical severity. *Brain Pathol* **19**, 596–611.
- 39 Volonte D, Liu Y & Galbiati F (2005) The modulation of caveolin-1 expression controls satellite cell activation during muscle repair. *FASEB J* **19**, 237–239.
- 40 Kim JE, Han JM, Park CR, Shin KJ, Ahn C, Seong JY & Hwang JI (2010) Splicing variants of the orphan G-protein-coupled receptor GPR56 regulate the activity of transcription factors associated with tumorigenesis. *J Cancer Res Clin Oncol* **136**, 47–53.
- 41 Taylor M, Treisman R, Garrett N & Mohun T (1989) Muscle-specific (CARG) and serum-responsive (SRE) promoter elements are functionally interchangeable in *Xenopus* embryos and mouse fibroblasts. *Development* **106**, 67–78.
- 42 Lawlor MW, Alexander MS, Viola MG, Meng H, Joubert R, Gupta V, Motohashi N, Manfready RA, Hsu CP, Huang P *et al.* (2012) Myotubularin-deficient myoblasts display increased apoptosis, delayed proliferation, and poor cell engraftment. *Am J Pathol* **181**, 961–968.
- 43 Gauthier-Rouviere C, Vandromme M, Tuil D, Lautredou N, Morris M, Soulez M, Kahn A, Fernandez A & Lamb N (1996) Expression and activity of serum response factor is required for expression of the muscle-determining factor MyoD in both dividing and differentiating mouse C2C12 myoblasts. *Mol Biol Cell* **7**, 719–729.
- 44 L'Honore A, Lamb NJ, Vandromme M, Turowski P, Carnac G & Fernandez A (2003) MyoD distal regulatory region contains an SRF binding CARG element required for MyoD expression in skeletal myoblasts and during muscle regeneration. *Mol Biol Cell* **14**, 2151–2162.
- 45 Zhang X, Azhar G, Helms S, Burton B, Huang C, Zhong Y, Gu X, Fang H, Tong W & Wei JY (2011) Identification of new SRF binding sites in genes modulated by SRF over-expression in mouse hearts. *Gene Regul Syst Bio* **5**, 41–59.
- 46 Horsley V, Friday BB, Matteson S, Kegley KM, Gephart J & Pavlath GK (2001) Regulation of the growth of multinucleated muscle cells by an NFATC2-dependent pathway. *J Cell Biol* **153**, 329–338.
- 47 Sakuma K, Nishikawa J, Nakao R, Watanabe K, Totsuka T, Nakano H, Sano M & Yasuhara M (2003) Calcineurin is a potent regulator for skeletal muscle regeneration by association with NFATc1 and GATA-2. *Acta Neuropathol* **105**, 271–280.
- 48 Cowling BS, McGrath MJ, Nguyen MA, Cottle DL, Kee AJ, Brown S, Schessl J, Zou Y, Joya J, Bonnemann CG *et al.* (2008) Identification of FHL1 as a regulator of skeletal muscle mass: implications for human myopathy. *J Cell Biol* **183**, 1033–1048.
- 49 Bahi-Buisson N, Poirier K, Boddaert N, Fallet-Bianco C, Specchio N, Bertini E, Caglayan O, Lascelles K, Elie C, Rambaud J *et al.* (2010) GPR56-related bilateral frontoparietal polymicrogyria: further evidence for an overlap with the cobblestone complex. *Brain* **133**, 3194–3209.
- 50 Carnac G, Primig M, Kitzmann M, Chafey P, Tuil D, Lamb N & Fernandez A (1998) RhoA GTPase and serum response factor control selectively the expression of MyoD without affecting Myf5 in mouse myoblasts. *Mol Biol Cell* **9**, 1891–1902.
- 51 Delling U, Tureckova J, Lim HW, De Windt LJ, Rotwein P & Molkenkin JD (2000) A calcineurin-NFATc3-dependent pathway regulates skeletal muscle differentiation and slow myosin heavy-chain expression. *Mol Cell Biol* **20**, 6600–6611.
- 52 Kegley KM, Gephart J, Warren GL & Pavlath GK (2001) Altered primary myogenesis in NFATC3(–/–) mice leads to decreased muscle size in the adult. *Dev Biol* **232**, 115–126.
- 53 Miano JM, Long X & Fujiwara K (2007) Serum response factor: master regulator of the actin cytoskeleton and contractile apparatus. *Am J Physiol Cell Physiol* **292**, C70–C81.
- 54 McCullagh KJ, Calabria E, Pallafacchina G, Ciciliot S, Serrano AL, Argentini C, Kalhovde JM, Lomo T & Schiaffino S (2004) NFAT is a nerve activity sensor in skeletal muscle and controls activity-dependent myosin switching. *Proc Natl Acad Sci USA* **101**, 10590–10595.
- 55 Calabria E, Ciciliot S, Moretti I, Garcia M, Picard A, Dyar KA, Pallafacchina G, Tothova J, Schiaffino S & Murgia M (2009) NFAT isoforms control activity-

- dependent muscle fiber type specification. *Proc Natl Acad Sci USA* **106**, 13335–13340.
- 56 Parrini E, Ferrari AR, Dorn T, Walsh CA & Guerrini R (2009) Bilateral frontoparietal polymicrogyria, Lennox-Gastaut syndrome, and GPR56 gene mutations. *Epilepsia* **50**, 1344–1353.
- 57 Talts JF, Andac Z, Gohring W, Brancaccio A & Timpl R (1999) Binding of the G domains of laminin alpha1 and alpha2 chains and perlecan to heparin, sulfatides, alpha-dystroglycan and several extracellular matrix proteins. *EMBO J* **18**, 863–870.
- 58 Saito F, Blank M, Schroder J, Manya H, Shimizu T, Campbell KP, Endo T, Mizutani M, Kroger S & Matsumura K (2005) Aberrant glycosylation of alpha-dystroglycan causes defective binding of laminin in the muscle of chicken muscular dystrophy. *FEBS Lett* **579**, 2359–2363.
- 59 Iyer D, Chang D, Marx J, Wei L, Olson EN, Parmacek MS, Balasubramanyam A & Schwartz RJ (2006) Serum response factor MADS box serine-162 phosphorylation switches proliferation and myogenic gene programs. *Proc Natl Acad Sci USA* **103**, 4516–4521.
- 60 Vandromme M, Gauthier-Rouviere C, Carnac G, Lamb N & Fernandez A (1992) Serum response factor p67SRF is expressed and required during myogenic differentiation of both mouse C2 and rat L6 muscle cell lines. *J Cell Biol* **118**, 1489–1500.
- 61 Megeney LA, Kablar B, Garrett K, Anderson JE & Rudnicki MA (1996) MyoD is required for myogenic stem cell function in adult skeletal muscle. *Genes Dev* **10**, 1173–1183.
- 62 Yablonka-Reuveni Z, Rudnicki MA, Rivera AJ, Primig M, Anderson JE & Natanson P (1999) The transition from proliferation to differentiation is delayed in satellite cells from mice lacking MyoD. *Dev Biol* **210**, 440–455.
- 63 Pearce JM, Pennington RJ & Walton JN (1964) Serum enzyme studies in muscle disease. III. Serum creatine kinase activity in relatives of patients with the Duchenne type of muscular dystrophy. *J Neurol Neurosurg Psychiatry* **27**, 181–185.
- 64 Nichol CJ (1965) Serum creatine phosphokinase measurements in muscular dystrophy studies. *Clin Chim Acta* **11**, 404–407.
- 65 Chan YM, Keramaris-Vrantsis E, Lidov HG, Norton JH, Zinchenko N, Gruber HE, Thresher R, Blake DJ, Ashar J, Rosenfeld J *et al.* (2010) Fukutin-related protein is essential for mouse muscle, brain and eye development and mutation recapitulates the wide clinical spectrums of dystroglycanopathies. *Hum Mol Genet* **19**, 3995–4006.
- 66 Schiaffino S & Reggiani C (1994) Myosin isoforms in mammalian skeletal muscle. *J Appl Physiol* **77**, 493–501.
- 67 Wigmore PM & Duglison GF (1998) The generation of fiber diversity during myogenesis. *Int J Dev Biol* **42**, 117–125.
- 68 Sanes JR (1982) Laminin, fibronectin, and collagen in synaptic and extrasynaptic portions of muscle fiber basement membrane. *J Cell Biol* **93**, 442–451.
- 69 Liesi P (1985) Do neurons in the vertebrate CNS migrate on laminin? *EMBO J* **4**, 1163–1170.
- 70 Hunter DD, Linas R, Ard M, Merlie JP & Sanes JR (1992) Expression of S-laminin and laminin in the developing rat central nervous system. *J Comp Neurol* **323**, 238–251.
- 71 Sanes JR (2003) The basement membrane/basal lamina of skeletal muscle. *J Biol Chem* **278**, 12601–12604.
- 72 Sasse J, von der Mark H, Kuhl U, Dessau W & von der Mark K (1981) Origin of collagen types I, III, and V in cultures of avian skeletal muscle. *Dev Biol* **83**, 79–89.
- 73 Wu MP & Gussoni E (2011) Carbamylated erythropoietin does not alleviate signs of dystrophy in mdx mice. *Muscle Nerve* **43**, 88–93.
- 74 Springer ML & Blau HM (1997) High-efficiency retroviral infection of primary myoblasts. *Somat Cell Mol Genet* **23**, 203–209.
- 75 Livak KJ & Schmittgen TD (2001) Analysis of relative gene expression data using real-time quantitative PCR and the 2(-Delta Delta C(T)) method. *Methods* **25**, 402–408.
- 76 Nolan T, Hands RE & Bustin SA (2006) Quantification of mRNA using real-time RT-PCR. *Nat Protoc* **1**, 1559–1582.
- 77 Silva JP, Lelianova V, Hopkins C, Volynski KE & Ushkaryov Y (2009) Functional cross-interaction of the fragments produced by the cleavage of distinct adhesion G-protein-coupled receptors. *J Biol Chem* **284**, 6495–6506.
- 78 Doyle JR, Fortin JP, Beinborn M & Kopin AS (2012) Selected melanocortin 1 receptor single-nucleotide polymorphisms differentially alter multiple signaling pathways. *J Pharmacol Exp Ther* **342**, 318–326.

## Supporting information

Additional supporting information may be found in the online version of this article at the publisher's web site:

**Fig. S1.** GPR56 localization at the membrane of primary wild-type myoblasts undergoing differentiation (day 2).

**Fig. S2.** Myosin heavy chain staining of muscle tissue.

**Table S1.** Quantitative RT-PCR primer sequences and concentrations.